Pseudo-labeling strategy and U-Net for high-resolution LULC mapping using CBERS-04A imagery in the Servidão river basin, Brazil

Danilo Marques de Magalhães[1], Murilo Marinho Pardo Lucas[1], Edgar Auler Galvão de França[2]

[1] Dept. of Geography and Environmental Planning, São Paulo State University, Rio Claro, Brazil – danilo.magalhaes@unesp.br, murilo.marinho@unesp.br
[2] Institute of Computing, University of Campinas, Campinas, Brazil – edgargalvaox@gmail.com

Keywords: Land use and land cover, U-Net, CBERS 04A, Pseudo-Labeling, Spectral Index, Principal Components Analysis.

Abstract

Accurate Land Use and Land Cover (LULC) data are vital for effective land planning and management. This study evaluates the U-Net model for LULC mapping using high-spatial-resolution (2 m) imagery from the WPM sensor on the CBERS 04A satellite. The research focuses on the Servidão River Basin in Rio Claro, Brazil, an urban watershed susceptible to flooding. A pseudo-labeling framework is proposed to reduce reliance on manually annotated training data. Training samples were automatically generated by integrating spectral indices (NDVI, NDWI, SOCI, CI, NISI), Principal Component Analysis, and unsupervised Iso-Cluster classification. Several U-Net configurations were evaluated, with a ResNet-34 backbone with class weighting achieving the highest performance. The model was then retrained using a manually refined reference dataset to enhance the representation of spectrally complex classes. Accuracy assessment resulted in an Overall Accuracy of 0.93, average Precision and Recall of 0.92, and a mean Intersection over Union (IoU) of 0.86. These findings indicate that the proposed pseudo-labeling strategy, combined with a U-Net, offers a robust approach for LULC mapping in complex urban environments using freely available CBERS 04A imagery.

1. Introduction

Land Use and Land Cover (LULC) data are essential for analyzing anthropogenic dynamics and environmental processes, and have been widely employed since the advent of orbital systems for terrestrial target classification and multitemporal monitoring (Bischof et al., 1992; Civco, 1993; Lou et al., 2024; Moran, 2010; Odenyo and Pettryt, 1977). The significance of LULC data extends across diverse fields, including climate emergency research (Wang et al., 2022), biodiversity loss (Dingamo et al., 2023; Sharma Arvind K., 2022), urban planning (Son et al., 2023), agricultural management (Tassis et al., 2021), geomorphological risk analysis (Pacheco Quevedo et al., 2023; Tyagi et al., 2023), and environmental planning and monitoring (Merino et al., 2024; Nery et al., 2024), among other terrestrial phenomena.

Technological advancements in remote sensing, particularly in spatial, spectral, temporal, and radiometric resolution, have improved efficiency (Holik et al., 2023), accuracy (Nigar et al., 2024), spatial coverage (Venter and Sydenham, 2021), and the overall capacity for large-scale data acquisition and analysis (Li et al., 2023; Lou et al., 2024; Lv et al., 2025; Parente et al., 2019; Sedona et al., 2019). However, these advances also increase the complexity of data processing, especially in environments with spectrally similar features, posing challenges for classification and interpretation (Abdollahi et al., 2021; Li et al., 2024; Roy et al., 2025; Yu et al., 2022). Therefore, effective classification, pattern detection, and modeling require the adoption of robust algorithms capable of managing such complexity (Li et al., 2024; Roy et al., 2025).

Deep Learning (DL) techniques have been successfully utilized to extract information from remote sensing images, especially in complex environments where different features exhibit spectral similarity (Carranza-García et al., 2019; Jozdani et al., 2019; Magalhães et al., 2025; Nigar et al., 2024; Vali et al., 2020). The rise in supervised classification accuracy and the widespread use of Graphics Processing Units (GPUs) to handle large datasets (Chopra, 2024) have been key factors driving DL research in remote sensing over the last five years (Victor et al., 2025).

Among DL models for remote sensing image classification, U-Net, a type of Convolutional Neural Network (CNN) developed for semantic segmentation, has become widely adopted (Solórzano et al., 2021). The U-Net architecture employs an encoder–decoder structure in which convolution and pooling operations extract hierarchical features, while upsampling restores spatial resolution. A defining feature is the use of skip connections that transfer information between corresponding encoding and decoding layers, thereby preserving spatial detail and enhancing segmentation accuracy (Vali et al., 2020; Wagner et al., 2020; Yan et al., 2022). Data augmentation methods, including rotations and mirroring, further improve model robustness (Yu et al., 2017).

To enhance feature extraction, U-Net is frequently integrated with backbone architectures such as ResNet, a deep residual network introduced by He et al. (2016). ResNet mitigates the degradation problem in very deep neural networks by incorporating residual (skip) connections, which enable the network to learn residual mappings rather than direct transformations. This approach improves gradient propagation across layers during training and supports the use of much deeper architectures without compromising performance. Consequently, ResNet is widely adopted as an encoder for semantic segmentation, offering robust multi-scale feature representations that strengthen the U-Net decoding stage.

Current research highlights the importance of customizing DL models for high-resolution image classification due to the variability in imagery and regional differences. Despite the flexibility of DL architectures, acquiring labeled data is challenging due to the substantial manual effort required, as noted by Li et al. (2024), Vali et al. (2020), and Yu et al. (2022).

This contribution has been peer-reviewed. The double-blind peer-review was conducted on the basis of the full paper.
https://doi.org/10.5194/isprs-annals-XI-3-2026-61-2026

Magalhães et al. (2025), for example, showed that U-Net outperforms traditional algorithms such as Random Forest and SVM for urban LULC mapping using high-resolution CBERS 04A imagery, but the need for manual labeling remains a significant obstacle to scaling this approach.

To address this limitation, recent studies have explored pseudo-labeling strategies in which unsupervised or weakly supervised methods generate initial labels when data are scarce. These approaches have yielded promising results for LULC by enabling models to learn spatial patterns and improve labels without extensive manual annotation (Wei et al., 2022; Zhang et al., 2024; Kim and Kim, 2024; Mirpulatov et al., 2023).

Accordingly, this study evaluates a pseudo-labeling strategy combined with a U-Net model for LULC mapping using high-resolution imagery from the WPM (Wide Panchromatic and Multispectral) sensor on the CBERS 04A (China–Brazil Earth Resources Satellite 04A). The proposed approach generates training data from spectral indices and uses Principal Component Analysis (PCA) and unsupervised classification methods to reduce reliance on manually annotated datasets. Model performance is assessed using independently generated reference data. Accurate, up-to-date, and high-resolution LULC data are critical for environmental and territorial planning, particularly for managing flood-prone areas in urbanized watersheds of Brazilian municipalities.

2. Study Area

The study area is the Servidão River basin, situated in the municipality of Rio Claro, within the interior of São Paulo State, Brazil (Figure 1).

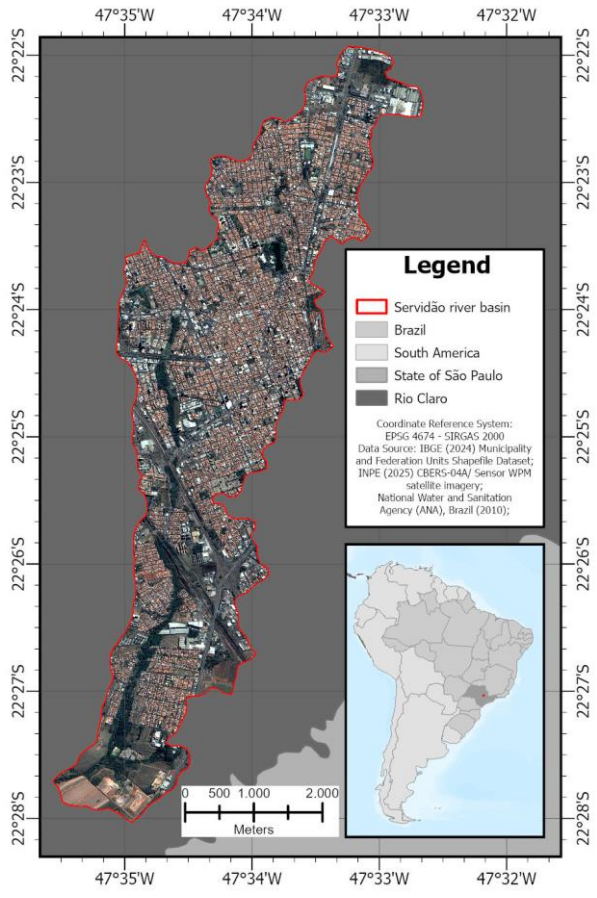

Figure 1. Location of study area.

The approximately 1,900-hectare watershed is mainly urbanized, with residential, commercial, and limited industrial use. In the southern portion, where urban and rural areas meet, a mosaic of exposed soil and herbaceous to arboreal vegetation is observed, especially along the partially preserved main channel bed.

In the central sector, where most of the urban area is concentrated, the main riverbed was channelized and covered in the 1970s, becoming a major city access route, reflecting national territorial management trends of the time (Moraes et al., 2012).

Urban expansion has rendered a significant portion of the basin impermeable, leading to increased surface runoff, reduced infiltration, and elevated peak flows (Tucci, 1997). In conjunction with the basin’s morphology, these conditions intensify local flooding (Schmidt, 2012). Additionally, the loss of vegetation, occupation of floodplains, and channelization further aggravate flooding, resulting in frequent floods and flash floods (Moruzzi et al., 2007), especially since the late twentieth century, when urban expansion accelerated (Moraes, 2011).

The municipality has a humid subtropical climate, with dry winters and hot, rainy summers (Alvares et al., 2013). The rainy season lasts from October to March (average 1200 mm), while the dry season runs from April to September (180–200 mm/year) (Troppmair, 1992).

3. Materials and Methods

The framework is based on a pseudo-labeling strategy, in which initial training data are automatically generated from spectral information and subsequently refined using DL techniques, reducing dependence on manually annotated datasets while enabling the extraction of spatial patterns from high-resolution imagery. The methodological approach comprised database preparation, training data generation, model training with a U-Net architecture, and accuracy assessment using standard metrics, all implemented in ArcGIS Pro 3.5 using built-in tools and custom ArcPy scripts.

Images acquired from the WPM sensor of the CBERS 04A satellite, provided by the Image Generation Division (*Divisão de Geração de Imagens* – DIDGI) of the National Institute for Space Research (*Instituto Nacional de Pesquisas Espaciais* – INPE), were used. These images include four spectral bands (RGB and NIR) at 8 m spatial resolution and a panchromatic band at 2 m spatial resolution. Spatial resolution was improved through pansharpening using the Brovey transformation with sensor-specific weights (Klippel, 2021), which was selected for its compatibility with CBERS 04A WPM data and its ability to preserve spatial detail and spectral contrast relevant to urban feature delineation, as demonstrated in previous studies (Magalhães et al., 2025).

Due to the lack of ground-truth data for model training, a pseudo-labeling strategy was implemented using spectral indices, PCA (Byrne et al., 1980), and unsupervised classification via the Iso-Cluster algorithm. This limitation applies only to the training phase; for validation, an independent reference dataset was produced through manual interpretation.

The Normalized Difference Vegetation Index (NDVI) (Rouse et al., 1973) was calculated to identify Dense Vegetation and Low Grass, which masked vegetated areas. Normalized Difference Water Index (NDWI) (McFeeters, 1996) was then applied to

This contribution has been peer-reviewed. The double-blind peer-review was conducted on the basis of the full paper.
https://doi.org/10.5194/isprs-annals-XI-3-2026-61-2026 | © Author(s) 2026. CC BY 4.0 License.

extract water bodies, resulting in an image primarily composed of urban features and exposed soils. To further distinguish among these classes, the Soil Organic Carbon Index (SOCI) (Minhoni et al., 2021), Coloration Index (CI) (Mandal, 2016), and Normalized Impervious Surface Index (NISI) (Su et al., 2022) were computed, as they are compatible with WPM. The corresponding formulas are provided in Equations 01 to 05.

$$NDVI = \frac{(NIR - RED)}{(NIR + RED)} \quad (1)$$

$$NDWI = \frac{(GREEN - NIR)}{(GREEN + NIR)} \quad (2)$$

$$SOCI = \frac{BLUE}{(RED \times GREEN)} \quad (3)$$

$$CI = \frac{(RED - GREEN)}{(RED + GREEN)} \quad (4)$$

$$NISI = \frac{(BLUE + GREEN + RED) - NIR}{(BLUE + GREEN + RED) + NIR} \quad (5)$$

The outputs of SOCI, CI, and NISI were integrated using PCA, with the first three components selected to minimize redundancy among spectral indices and retain the most relevant information. These components capture most of the data variance while preserving dominant spectral patterns (Jolliffe, 2002; Richards, 2013; Lillesand et al., 2015) and are compatible with the input requirements of the subsequent unsupervised classification, which operates up to three bands. An unsupervised Iso-Cluster classification was then performed (Figure 2), producing an initial raster with five predominant LULC classes: asphalt, fiber-cement and ceramic roofs, concrete slabs, and exposed soils. This result was then merged with additional classes derived from spectral indices, specifically Dense Vegetation and Low Grass from the NDVI, and Water from the NDWI, resulting in a final pseudo-label dataset comprising eight LULC classes for model training.

This dataset was employed as pseudo-label reference data for training the U-Net model. A total of seven models were developed across three sequential stages: an initial training phase (Models A–D), a second phase with adjusted input parameters (Models E–F), and a final retraining phase using refined reference data (Model G). Class imbalance among LULC classes was considered during model training. To address this issue, experiments were conducted both with and without class weighting, enabling the assessment of its influence on model performance.

During the first round, four models were trained using 256×256 tiles: (A) ResNet-34 without class weighting, (B) ResNet-34 with class weighting, (C) ResNet-50 without class weighting, and (D) ResNet-50 with class weighting. Model selection was guided by qualitative assessment of segmentation consistency and reduction of misclassification patterns. Models trained with ResNet-34 showed the best performance, particularly Model B, leading to the exclusion of ResNet-50 models.

In the second round, two models (E and F) were trained on 512×512 tiles using ResNet-34, without and with class weighting, respectively. Although these models produced satisfactory results, they exhibited higher commission errors than Model B. Therefore, Model B was chosen for further analysis.

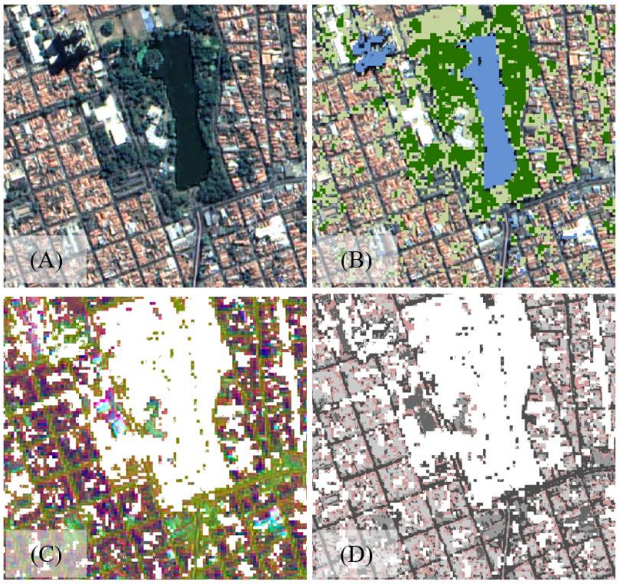

Figure 2. Workflow for generating pseudo-labels used in model training. (A) RGB CBERS 04A image. (B) Dense Vegetation (dark green) and Low Grass (light green) derived from NDVI, and Water (blue) derived from NDWI. (C) PCA derived from the spectral indices SOCI, CI, and NISI. (D) Iso-Cluster classification, representing five LULC classes (from darkest grey to lightest: Asphalt, Fiber Cement, Concrete, and Ceramic; Bare Soil in pink).

Model B was trained using a ResNet-34 backbone with randomly initialized weights, a batch size of 8, and a chip size of 256×256 pixels. Training was conducted for up to 200 epochs, with early stopping based on validation loss to prevent overfitting, resulting in 54 training epochs. A learning rate ranging from 1.3×10^{-5} to 1.3×10^{-4} was adopted, and 10% of the dataset was reserved for validation. Class balancing was enabled, and the loss function incorporated focal loss, while dice loss was not applied. Data augmentation included random cropping, dihedral affine transformations (rotations and reflections), and adjustments in brightness, contrast, and zoom, following the default configuration of the ArcGIS Pro DL framework (ESRI, 2025). The model was fully trainable (no layer freezing), and performance was monitored using validation loss.

Model B successfully mapped eight LULC classes, including Dense Vegetation, Low Grass, Water, Asphalt, Fiber-Cement Roofs, Ceramic Roofs, Concrete, and Bare Soil. Shadows and Cemetery were not identified, as these classes were not present in the pseudo-labels. Shadows were often misclassified as water, and cemeteries as concrete or fiber-cement roofs. To enhance classification consistency, the map was manually corrected by adjusting class attributes without further vectorization or topological editing. This corrected map served as the reference for retraining the model, leading to the final version, Model G, which retained the same ResNet-34 architecture with class weighting.

Model G’s results were evaluated using standard remote sensing metrics: Overall Accuracy (OA), Precision, Recall, F1-Score, and Intersection over Union (IoU) (Maxwell et al., 2021a; 2021b), as well as a confusion matrix. Reference data for accuracy assessment were generated independently by manual interpretation to ensure an unbiased assessment. A stratified probabilistic sampling scheme (Tyukavina et al., 2025) was

https://doi.org/10.5194/isprs-annals-XI-3-2026-61-2026

implemented, with a minimum of 5% samples per class, resulting in 1,324 polygons covering 132.67 ha (Table 1).

Class	Predicted Area (ha)	Sampled Area (ha)	Sampled Area (%)	Polygon Count
Dense Vegetation	217.5092	25.0628	11.52	58
Low Grass	379.9872	26.156	6.88	94
Asphalt	470.2356	23.8863	5.08	301
Fiber Cement	204.6148	11.454	5.60	85
Concrete	61.6572	5.3851	8.73	97
Ceramic	409.0008	21.2356	5.19	468
Shadows	50.1604	2.9575	5.90	113
Cemetery	5.7564	2.2887	39.76	19
Bare Soil	101.5896	12.3385	12.15	76
Water	4.2808	1.9135	44.70	13
Total	1,904.792	132.678	6.97%	1,324

Table 1. Distribution of samples for accuracy verification in relation to the total LULC of the watershed.

Figure 3 summarizes the methodological workflow, from pseudo-label generation to model training and accuracy assessment.

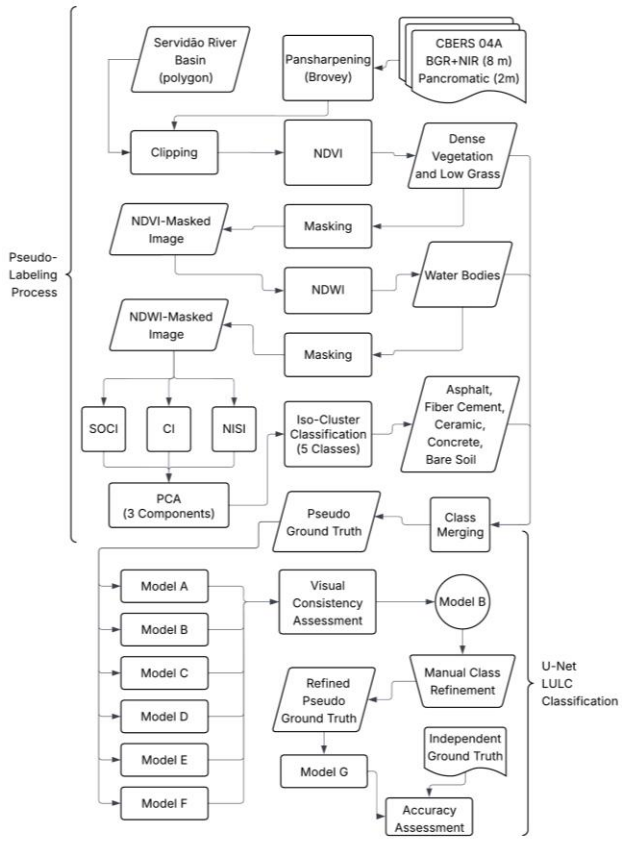

Figure 3. Adopted methodology workflow including pseudo-label generation, U-Net model training, and accuracy assessment.

All datasets and processing resources utilized in this study are publicly available in a GitHub repository (https://github.com/mapearunesp-bit). These resources include the CBERS 04A imagery, the pseudo-label dataset, the refined reference data, and the independently generated ground truth for accuracy assessment. The repository also contains the ModelBuilder workflow implemented with native ArcGIS Pro tools, the ArcPy script developed for accuracy assessment, and the complete methodological workflow described in this study.

4. Results

The results indicate that the U-Net model demonstrates satisfactory performance in segmenting the primary LULC classes identified in the Servidão river basin using the WPM image from CBERS 04A. The model achieved high accuracy across all performance evaluation metrics (Table 2), reflecting strong agreement between Model G predictions and independently derived ground truth data. The consistent average Precision, Recall, and F1-Score (0.92) suggest minimal bias between commission and omission errors, indicating that both the model architecture and the dataset are suitable for distinguishing the observed targets, even within the spectrally and spatially complex urban environment analyzed.

Metric	OA	Precision	Recall	F1-Score	IoU
Result	0.93	0.92	0.92	0.92	0.86

Table 2. Overall accuracy assessment. The table reports mean values derived from the evaluation of each class.

Class-specific analysis reveals patterns that align with the inherent complexity of the scene, which results from substantial spatial information and the spectral limitations of the visible and near-infrared bands (Table 3). Most segmentation results are excellent, with many metrics exceeding 0.9, underscoring the U-Net model's effectiveness in precise object segmentation from high-resolution remote sensing imagery. Lower performances are noted for the Fiber-Cement Roofs and Shadows classes, likely due to their similar spectral and textural characteristics, as both exhibit dark coloration and homogeneous textures. In contrast, classes such as Ceramic Roofs and Bare Soil, despite their similar spectral signature, exhibit distinct textures, which may explain the model's ability to distinguish between them. Notably, Shadows were mapped solely to prevent misclassification as other classes (e.g., Fiber Cement) and should be reclassified in future applications to ensure proper representation in the LULC map.

Class	Precision	Recall	F1 Score	IoU
Dense Vegetation	0.93	0.97	0.95	0.91
Low Grass	0.93	0.93	0.93	0.87
Asphalt	0.93	0.96	0.94	0.89
Fiber Cement	0.89	0.86	0.87	0.77
Concrete	0.94	0.86	0.90	0.81
Ceramic	0.98	0.97	0.97	0.95
Shadows	0.64	0.81	0.71	0.56
Cemetery	1.00	0.99	1.00	0.99
Bare Soil	0.99	0.88	0.93	0.87
Water	0.99	0.97	0.98	0.96

Table 3. Accuracy assessment by class.

The confusion matrix presented in Figure 4 provides additional insight by comparing Model G's predictions with independently derived ground-truth data. Cell colors are normalized by row to correspond with ground-truth classes, thereby facilitating class-wise performance assessment. The main diagonal represents True Positives (TP). Model G demonstrates high accuracy across most classes, including underrepresented classes such as Water and Cemetery. This outcome might indicate that class imbalance did not significantly influence the model performance.

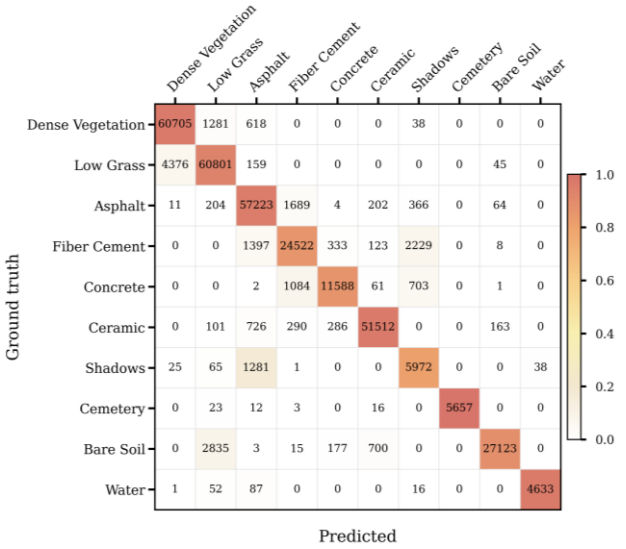

Figure 4. Confusion matrix for LULC classification. Cell colors indicate row-normalized values, and numbers show pixel counts, allowing class-wise performance comparison despite class imbalance.

Most classification errors occur among prevalent and spectrally similar classes, particularly between Low Grass and Dense Vegetation, Fiber Cement and Shadows and Asphalt, Shadows and Asphalt, and Bare Soil and Low Grass.

The confusion between Low Grass and Dense Vegetation likely results from variations in vegetative vigor. Some low-grass areas exhibited high NDVI values, possibly due to increased plant height or artificial irrigation, such as in soccer fields. The misclassification between Bare Soil and Low Grass reflects both spectral similarity and spatial proximity, especially in rural areas where narrow access paths intersect pasture. Although Asphalt is typically identified by its dark coloration, homogeneous texture, and elongated shapes, misclassifications with Fiber Cement persist. These errors are likely due to their similarities in reflectance patterns. Overall, these results indicate that classification errors are more strongly associated with spectral similarity than with class imbalance.

Despite the pseudo ground-truth's characteristics, U-Net Model G achieved satisfactory segmentation accuracy. The improvement observed demonstrates that the DL model goes beyond simply replicating the initial pseudo-labels; it refines class boundaries and corrects inconsistencies by learning spatial patterns. This highlights the model’s ability to enhance initial representations from spectral indices and unsupervised classification, reducing dependence on manual labeling.

It is important to note that the results may be affected by inherent limitations of the Brovey pansharpening process, and modifications or the use of alternative methods could further improve accuracy. Although spatial detail is enhanced to 2 m, this enhancement does not generate spectrally independent information at that resolution. The spectral content is primarily determined by the original 8 m multispectral data and is spatially redistributed during fusion. Therefore, variations observed at the 2 m pixel level represent a spatial interpolation of the spectral response, indicating gradual transitions within the area corresponding to the original 8 m pixels.

Figure 5 illustrates the reference data generation steps and the segmentation by Models B and G, showing improved segmentation over the initial pseudo ground truth.

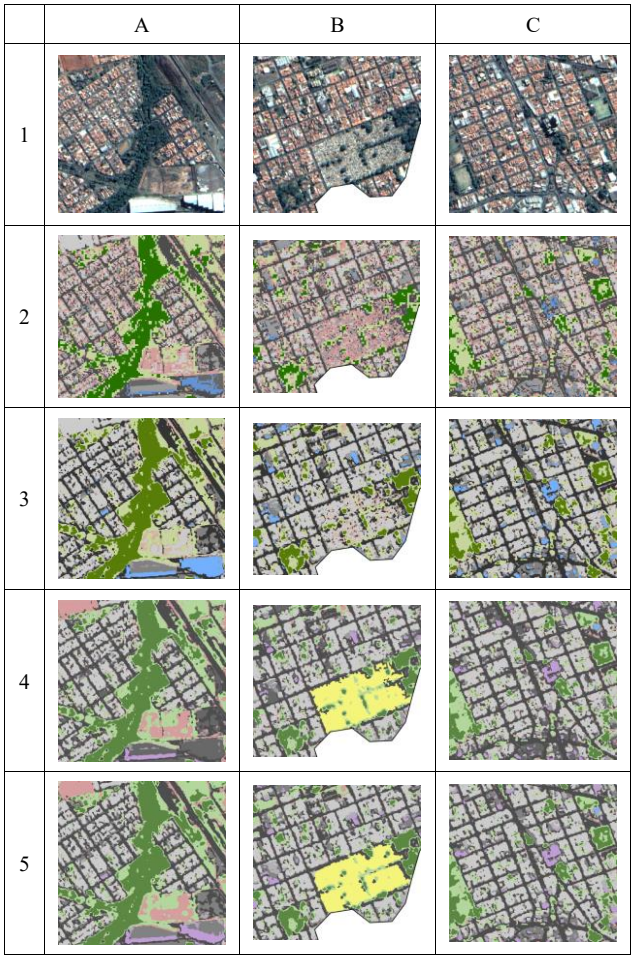

Figure 5. Stages of LULC classification workflow. The columns show different areas which highlight (A) Dense Vegetation, Low Grass and Bare Soil; (B) Cemetery; (C) Urbanized areas. Row 1: CBERS 04A RGB image. Row 2: pseudo-label dataset generated from spectral indices, PCA, and Iso-Cluster classification. Row 3: initial segmentation produced by Model B, highlighting misclassification patterns (e.g., shadows classified as water and omission of the cemetery). Row 4: manually corrected reference dataset derived from Model B. Row 5: segmentation generated by Model G.

5. Conclusions

This study evaluated the technical feasibility of a pseudo-labeling strategy based on spectral indices and PCA, combined with a U-Net model with a ResNet-34 backbone implemented in ArcGIS Pro, for high-resolution LULC mapping using CBERS 04A (WPM) imagery. The proposed approach substantially reduced the requirement for manual data labeling while maintaining high classification accuracy and delivering precise spatial delineation of LULC features.

The proposed methodology enabled accurate segmentation of the primary LULC classes present in both urban and rural areas. These findings demonstrate the effectiveness of the U-Net model in segmenting features within high-resolution remote sensing imagery, even under conditions of significant class heterogeneity and limited spectral bands. The most substantial classification challenges arose with targets exhibiting dark

This contribution has been peer-reviewed. The double-blind peer-review was conducted on the basis of the full paper.
https://doi.org/10.5194/isprs-annals-XI-3-2026-61-2026 | © Author(s) 2026. CC BY 4.0 License.

coloration and homogeneous texture, such as shadows, fiber-cement roofs, and asphalt. Future improvements may involve increasing the quantity of labeled input data or incorporating additional information into model training, such as the spectral indices and PCA generated in this study.

The methodological framework employed in this study is based on widely adopted remote sensing techniques, which ensure reproducibility and adaptability across different sensors and scene classifications. This research demonstrates that pseudo-labeling strategies facilitate information extraction from high-resolution imagery using deep learning models. These strategies reduce dependence on manually labeled data, a significant challenge identified in the literature, and support LULC mapping in complex environments, including heterogeneous urban areas.

While the combination of spectral indices, PCA, and Iso-Cluster provided satisfactory pseudo-ground-truth data, manual adjustments to certain attributes and reprocessing of the model enabled the inclusion of new classes and further improved results. Therefore, when replicating this methodology, it is important to consider the additional effort these adjustments may entail, particularly for large-scale mapping.

Based on these results, subsequent experiments will evaluate the model’s ability to generalize across images from the same sensor and location on different dates, aiming to develop a LULC time series. Future studies will also evaluate alternative pansharpening approaches, particularly those based on CNNs, as they are expected to preserve spectral information better and, consequently, enhance classification performance.

The ongoing research will also automate the framework using Model Builder and the ArcPy environment within ArcGIS Pro, with the goal of producing LULC time series for the entire municipality of Rio Claro. These results have the potential to improve monitoring of territorial transformations in Brazilian municipalities by utilizing free, high-resolution data collected by a domestically produced satellite.

Acknowledgements

The authors acknowledge the São Paulo Research Foundation (FAPESP), Brazil (Grant 2025/11196-0).

References

Abdollahi, A., Pradhan, B., Shukla, N., Chakraborty, S., Alamri, A., 2021. Multi-object segmentation in complex urban scenes from high-resolution remote sensing data. *Remote Sens.* 13. https://doi.org/10.3390/rs13183710

Alvares, C.A., et al., 2013: Köppen’s climate classification map for Brazil. *Meteorol. Z.*, 22(6), 711–728.

Bischof, H., Schneider, W., Pinz, A.J., 1992. Multispectral Classification of Landsat-Images Using Neural Networks. *IEEE Transactions on Geocience and Remote Sens.,* 30, 482–490. http://doi.org/10.1109/36.142926

Byrne, G.F., Crapper, P.F., Mayo, K.K., 1980. Monitoring land-cover change by principal component analysis of multitemporal Landsat data. *Remote Sens. Environ*. 10(3), 175–184. https://doi.org/10.1016/0034-4257(80)90021-8

Carranza-García, M., García-Gutiérrez, J., Riquelme, J.C., 2019. A framework for evaluating land use and land cover classification using convolutional neural networks. *Remote Sens.* 11. https://doi.org/10.3390/rs11030274

Chopra, B., 2024. Enhancing Machine Learning Performance: The Role of GPU-Based AI Compute Architectures. *Journal of Knowledge Learning and Science Technology.* ISSN: 2959-6386 (online) 3, 20–32. https://doi.org/10.60087/jklst.vol3.n3.p20-32

Civco, D.L., 1993. Artificial neural networks for land-cover classification and mapping. *International Journal of Geographical Information Systems* 7, 173–186. https://doi.org/10.1080/02693799308901949

Dingamo, T., Takele, S., Demissew, S., Woldu, Z., 2023. Evaluate and analyze land cover change dynamics, driving force and their implications to biodiversity in the western escarpment of the Rift valley. *Land Degrad Dev* 34, 5017–5028. https://doi.org/10.1002/ldr.4826

ESRI, 2025. Train Deep Learning Model (Image Analyst) — ArcGIS Pro Tool Reference. https://pro.arcgis.com/en/pro-app/latest/tool-reference/image-analyst/train-deep-learning-model.htm. (14 November 2025).

He, K., Zhang, X., Ren, S., Sun, J., 2016. Deep residual learning for image recognition. In: *Proceedings of the IEEE Conference on Computer Vision and Pattern Recognition* (CVPR), 770–778. https://doi.org/10.1109/CVPR.2016.90

Holik, A., Erwanto, Z., Hardiyanti, S., 2023. Google Earth Engine for Assessing Land Use and Land Cover Change in Banyuwangi Regency. *INSTICC*, pp. 416–422. https://doi.org/10.5220/0010946800003260

Jolliffe, I.T., 2002. *Principal Component Analysis*. Springer.

Jozdani, S.E., Johnson, B.A., Chen, D., 2019. Comparing deep neural networks, ensemble classifiers, and support vector machine algorithms for object-based urban land use/land cover classification. *Remote Sens.* 11. https://doi.org/10.3390/rs11141713

Kim, J., Kim, Y., 2024. Integrated Framework for Unsupervised Building Segmentation with Segment Anything Model-Based Pseudo-Labeling and Weakly Supervised Learning. *Remote Sens.*, 16(3), 526. https://doi.org/10.3390/rs16030526

Klippel, S., 2021. CBERS 04A Downloader QGIS Plugin. https://github.com/sandroklippel/cbers4a (11 November 2025).

Li, Z., Chen, B., Wu, S., Su, M., Chen, J.M., Xu, B., 2024. Deep learning for urban land use category classification: A review and experimental assessment. *Remote Sens. Environ.* 311 https://doi.org/10.1016/j.rse.2024.114290

Li, Z., He, W., Cheng, M., Hu, J., Yang, G., Zhang, H., 2023. SinoLC-1: The first 1m resolution national-scale land-cover map of China created with a deep learning framework and open-Access data. *Earth Syst Sci Data* 15, 4749–4780. https://doi.org/10.5194/essd-15-4749-2023

Lillesand, T., Kiefer, R.W., Chipman, J., 2015. *Remote Sens. and Image Interpretation*. Wiley.

Lou, C., Al-qaness, M.A.A., AL-Alimi, D., Dahou, A., Abd Elaziz, M., Abualigah, L., Ewees, A.A., 2024. Land use/land cover (LULC) classification using hyperspectral images: a review. *Geo-Spatial Information Science*. https://doi.org/10.1080/10095020.2024.2332638

Lv, Q., Qi, Z., Li, H., Song, W., Huang, D., Ding, Z., Shi, Q., 2025. Evaluating the potential of multi-source remote sensing and urban big data for urban land use classification. *Int J Digit Earth* 18. https://doi.org/10.1080/17538947.2025.2546519

Magalhães, D.M., Souza, J.P., França, E.A.G., 2025. Deep Learning for supervised classification of CBERS 04A imagery in Rio Claro (SP) urban area. *Revista Brasileira de Cartografia*, 77. https://doi.org/10.14393/rbcv77n0a-75495

Mandal, U.K., 2016. Spectral color indices based geospatial modeling of soil organic matter in Chitwan District, Nepal. In: International Archives of the Photogrammetry, Remote Sensing and Spatial Information Sciences - *ISPRS Archives. International Society for Photogrammetry and Remote Sensing*, pp. 43–48. https://doi.org/10.5194/isprsarchives-XLI-B2-43-2016

Maxwell, A.E., Warner, T.A., Guillén, L.A., 2021a. Accuracy assessment in convolutional neural network-based deep learning remote sensing studies—Part 1: Literature review. *Remote Sens.* 13, 2450. https://doi.org/10.3390/rs13132450

Maxwell, A.E., Warner, T.A., Guillén, L.A., 2021b. Accuracy assessment in convolutional neural network-based deep learning remote sensing studies—Part 2: Recommendations and best practices. *Remote Sens.* 13, 2591. https://doi.org/10.3390/rs13132591

McFeeters, S.K., 1996. The use of the Normalized Difference Water Index (NDWI) in the delineation of open water features. *Int. J. Remote. Sens.* 17, 1425–1432. https://doi.org/10.1080/01431169608948714

Merino, E.R., de Azevedo, D.A., Alvarez, M.O.T., da Silva Ramalho, A., 2024. Evaluating territorial management of integrated development region (RIDE-DF) and its effect on land use land cover transformation. *Journal of Maps* 20(1). https://doi.org/10.1080/17445647.2024.2395916

Minhoni, R.T. de A., Scudiero, E., Zaccaria, D., Saad, J.C.C., 2021. Multitemporal satellite imagery analysis for soil organic carbon assessment in an agricultural farm in southeastern Brazil. *Science of the Total Environment* 784. https://doi.org/10.1016/j.scitotenv.2021.147216

Mirpulatov, I., Illarionova, S., Shadrin, D., Burnaev, E., 2023. Pseudo-Labeling Approach for Land Cover Classification Through Remote Sensing Observations with Noisy Labels. *IEEE Access*, 11, 82570–82583. https://doi.org/10.1109/ACCESS.2023.3300967

Moraes, I.C., 2011. *Análise da dinâmica do uso da terra e sua interferência em inundações na cidade de Rio Claro (SP)* [Land use dynamics and its influence on flooding in the city of Rio Claro (SP)]. MSc Dissertation, Universidade Estadual Paulista (UNESP), Instituto de Geociências e Ciências Exatas, Rio Claro, SP, Brazil.

Moraes, I.C., Conceição, F.T., Cunha, C.M.L., Moruzzi, R.B. 2012. Interferência do uso da terra nas inundações da área urbana do córrego da Servidão, Rio Claro (SP) [Influence of land use on urban flooding in the Córrego da Servidão watershed, Rio Claro (SP)]. *Rev. Bras. Geomorfol.*, 13(2). https://doi.org/10.20502/rbg.v13i2.252

Moran, E.F., 2010. Land Cover Classification in a Complex Urban-Rural Landscape with Quickbird Imagery. *Photogramm Eng Remote Sensing* 76, 1159–1168. http://doi.org/10.14358/pers.76.10.1159

Moruzzi, R.B., Pinto, S.A.F, Rosseti, L.A.G., Pereira, L.H., Bermudez, M., Barbora, C., 2007. Contribuição metodológica para a caracterização de áreas potenciais de inundação em uma bacia hidrográfica urbanizada, com o suporte de técnicas de sensoriamento remoto e geoprocessamento: apresentação de dois cenários em um módulo piloto [Methodological contribution for identifying potential flood-prone areas in an urbanized watershed using remote sensing and GIS: a pilot module with two scenarios]. *Proc. XVII Simpósio Brasileiro de Recursos Hídricos*, São Paulo, Brazil.

Nery, L.M., Toniolo, B.P., dos Santos, A.P., Martins, A.C.G., da Cunha e Silva, D.C., 2024. Challenge of political integration in the territorial management of a protected area based on the analysis of land use and land cover change. *J Environ Stud Sci* 15, 845–860. https://doi.org/10.1007/S13412-024-00990-6

Nigar, A., Li, Y., Jat Baloch, M.Y., Alrefaei, A.F., Almutairi, M.H., 2024. Comparison of machine and deep learning algorithms using Google Earth Engine and Python for land classifications. *Front Environ Sci* 12. https://doi.org/10.3389/fenvs.2024.1378443

Odenyo, V.A.O., Pettryt, D.E., 1977. Land-Use Mapping by Machine Processing of LANDSAT-1 Data. *Photogramm Eng Remote Sensing* 43, 515–523.

Pacheco Quevedo, R., Velastegui-Montoya, A., Montalván-Burbano, N., Morante-Carballo, F., Korup, O., Daleles Rennó, C., 2023. Land use and land cover as a conditioning factor in landslide susceptibility: a literature review. *Landslides*. https://doi.org/10.1007/s10346-022-02020-4

Parente, L., Taquary, E., Silva, A.P., Souza, C., Ferreira, L., 2019. Next generation mapping: Combining deep learning, cloud computing, and big remote sensing data. *Remote Sens*. 11. https://doi.org/10.3390/rs11232881

Richards, J.A., 2013. *Remote Sensing Digital Image Analysis*. Springer.

Rouse, J.W., Haas, R.H., Schell, J.A., Deering, D.W., 1973. Monitoring vegetation systems in the Great Plains with ERTS, in: *Third ERTS Symposium*. NASA, Washington, DC, pp. 309–317.

Roy, K., Homayouni, S., Zhang, Y., 2025. Self-Supervised Deep Learning for Urban Land Cover Classification from Very High-Resolution Imagery. *Canadian Journal of Remote Sensing* 51. https://doi.org/10.1080/07038992.2025.2532528

Sedona, R., Cavallaro, G., Jitsev, J., Strube, A., Riedel, M., Benediktsson, J.A., 2019. Remote sensing big data classification with high performance distributed deep learning. *Remote Sens*. 11. https://doi.org/10.3390/rs11243056

Schmidt, K.C., 2012. *Efeitos da ocupação e uso da terra na bacia do córrego da Servidão, no cenário de 1995–2006* [Effects of land use and occupation on the Córrego da Servidão watershed, 1995–2006]. Undergraduate Thesis, Universidade Estadual Paulista (UNESP). https://repositorio.unesp.br/entities/publication/7c763e56-3be3-4a20-9a5a-acf38e6d9126 (14 November 2025)

Sharma, A.K., Sharma, A.K., Sharma, M., Sharma, M., 2022. Assessment of Land Use Change and Climate Change Impact on Biodiversity and Environment, in: Bahukhandi Kanchan Deoli and Kamboj, N. and K.V. (Ed.), *Environmental Pollution and Natural Resource Management*. Springer International Publishing, Cham, pp. 73–89. https://doi.org/10.1007/978-3-031-05335-1_5

Solórzano, J. V., Mas, J.F., Gao, Y., Gallardo-Cruz, J.A., 2021. Land use land cover classification with U-net: Advantages of combining sentinel-1 and sentinel-2 imagery. *Remote Sens*. 13. https://doi.org/10.3390/rs13183600

Son, T.H., Weedon, Z., Yigitcanlar, T., Sanchez, T., Corchado, J.M., Mehmood, R., 2023. Algorithmic urban planning for smart and sustainable development: Systematic review of the literature. *Sustain Cities Soc.* https://doi.org/10.1016/j.scs.2023.104562

Su, S., Tian, J., Dong, X., Tian, Q., Wang, N., Xi, Y., 2022. An Impervious Surface Spectral Index on Multispectral Imagery Using Visible and Near-Infrared Bands. *Remote Sens.* 14. https://doi.org/10.3390/rs14143391

Tassis, L.M., Tozzi de Souza, J.E., Krohling, R.A., 2021. A deep learning approach combining instance and semantic segmentation to identify diseases and pests of coffee leaves from in-field images. *Comput. Electron. Agric.* 186. https://doi.org/10.1016/j.compag.2021.106191

Troppmair, H., 1992. *Atlas da qualidade ambiental e de vida de Rio Claro-SP* [Environmental and Quality of Life Atlas of Rio Claro-SP]. UNESP, Rio Claro.

Tucci, C.E.M., 1997. Plano diretor de drenagem urbana: princípios e concepção [Urban drainage master plan: principles and design]. *Rev. Bras. Rec. Hídricos (RBRH)*, 2(2). Porto Alegre, RS. http://dx.doi.org/10.21168/rbrh.v2n2.p5-12

Tyagi, A., Tiwari, R.K., James, N., 2023. Prediction of the future landslide susceptibility scenario based on LULC and climate projections. Landslides 20, 1837–1852. https://doi.org/10.1007/s10346-023-02088-6

Tyukavina, A., Stehman, S.V., Pickens, A.H., Potapov, P., Hansen, M.C., 2025. Practical global sampling methods for estimating area and map accuracy of land cover and change. *Remote Sens. Environ.* 324, 114714. https://doi.org/10.1016/j.rse.2025.114714

Vali, A., Comai, S., Matteucci, M., 2020. Deep learning for land use and land cover classification based on hyperspectral and multispectral earth observation data: A review. *Remote Sens*. https://doi.org/10.3390/RS12152495

Venter, Z.S., Sydenham, M.A.K., 2021. Continental-scale land cover mapping at 10 m resolution over europe (Elc10). *Remote Sens.* 13. https://doi.org/10.3390/rs13122301

Victor, B., He, Z., Nibali, A., 2025. A systematic review of the use of Deep Learning in Satellite Imagery for Agriculture. *IEEE J. Sel. Top. Appl. Earth. Obs. Remote Sens.* 18, 2297–2316. https://doi.org/10.1109/JSTARS.2024.3501216

Wagner, F.H., Dalagnol, R., Casapia, X.T., Streher, A.S., Phillips, O.L., Gloor, E., Aragão, L.E.O.C., 2020. Regional mapping and spatial distribution analysis of Canopy palms in an Amazon forest using deep learning and VHR images. *Remote Sens.* 12. https://doi.org/10.3390/rs12142225

Wang, R., Wang, M., Zhang, Z., Hu, T., Xing, J., He, Z., Liu, X., 2022. Geographical Detection of Urban Thermal Environment Based on the Local Climate Zones: A Case Study in Wuhan, China. *Remote Sens.* 14. https://doi.org/10.3390/rs14051067

Wei, P., Huang, R., Lin, T., Huang, J., 2022. Rice Mapping in Training Sample Shortage Regions Using a Deep Semantic Segmentation Model Trained on Pseudo-Labels. *Remote Sens.*, 14(2), 328. https://doi.org/10.3390/rs14020328

Yan, C., Fan, X., Fan, J., Wang, N., 2022. Improved U-Net Remote Sensing Classification Algorithm Based on Multi-Feature Fusion Perception. *Remote Sens.* 14. https://doi.org/10.3390/rs14051118

Yu, J., Zeng, P., Yu, Y., Yu, H., Huang, L., Zhou, D., 2022. A Combined Convolutional Neural Network for Urban Land-Use Classification with GIS Data. *Remote Sens.* 14. https://doi.org/10.3390/rs14051128

Yu, X., Wu, X., Luo, C., Ren, P., 2017. Deep learning in remote sensing scene classification: a data augmentation enhanced convolutional neural network framework. GISci. *Remote Sens.* 54, 741–758. https://doi.org/10.1080/15481603.2017.1323377

Zhang, J., You, S., Liu, A., Xie, L., Huang, C., Han, X., Li, P., Wu, Y., Deng, J., 2024. Winter Wheat Mapping Method Based on Pseudo-Labels and U-Net Model for Training Sample Shortage. *Remote Sens.*, 16(14), 2553. https://doi.org/10.3390/rs16142553